A COMPARISON OF EMPIRICAL AND CFD-BASED EXERGY MODELLING FOR THE AIRFRAME SUBSYSTEM OF AIRCRAFT DESIGN

Ken Alabi[±], Michael von Spakovsky[ρ], Foluso Ladeinde*, David Moorhouse[**], and Jose Camberos[**]
[±]Thaerocomp Technical Corp. P. O. Box 1527, Stony Brook, NY 11790. USA
[ρ]Department of Mechanical Engineering 0238, Virginia Tech, Blacksburg, VA 24601. USA
*Thaerocomp Technical Corp. P. O. Box 1527, Stony Brook, NY 11790. USA
**Air Force Research Laboratory, Wright-Patterson Air Force Base, OH 45433-7542

Abstract

This paper compares empirical and computational fluid dynamics (CFD) - based exergy calculation procedures for modeling the airframe subsystem of aircraft. Calculations were based on the B747-200 aircraft, with the presumption that the empirical methods were valid. They were carried out for a range of values of the angle of attack, assuming transonic flight. Good agreement was observed for one approach, supporting the viability of using CFD for realistic airframe calculations in a system-level analysis and design optimization.

1 Introduction

The design of complete aircraft is a complicated undertaking consisting of a myriad of variables and requiring the convergence of technologies and experts from different disciplines. Engineers have tackled this problem by decomposing (e.g., [1-5]) the system along sub-system lines. In this sense, the system is composed of physically-interacting subsystems, each possessing a certain degree of autonomy but depending on other subsystems via a number of coupling or shared variables [1, 5-10].

For example, in [5,8,9], a decomposition strategy called dynamic iterative local-global optimization (DILGO) [10] is successfully applied to the synthesis/design of an advanced tactical fighter aircraft. This is accomplished by decomposing the aircraft into six subsystems: propulsion, fuel-loop, vapor compression and PAO loops, environmental control, airframe, and permanent/expendable payload and equipment group. In total, these subsystem models result in nearly 500 degrees of freedom of the optimization level, with a mix of both discrete and continuous decision variables. DILGO is employed for dynamically optimizing, in an integrated fashion *consistent with the optimum for the vehicle as a whole*, each of the subsystems' syntheses/designs while taking into account the optimal behavior of each subsystem at off-design, i.e. across an entire mission. This is done without the nesting of optimizations and, thus, much higher computational burden typical of local-global decomposition strategies found in the literature. This lack of nesting permits a degree of parallelization in the process of subsystem and system optimization not possible with other decomposition strategies.

With DILGO, even larger problems can be handled successfully. A complete aircraft design problem typically consists of many subsystems, including the Air Frame-Structural, Air Frame-Aerodynamics, Environmental Control, Propulsion, Vapor Compression / PAO Loops, Oil Loop, Electrical, Hydraulic, Fuel Loop, Expendable Payload, Equipment Group, Permanent Payload, and Controls. The current paper focuses on the aerodynamic synthesis/design of the air frame subsystem (AFS). One advantage of the multi-level or decomposition approach is that it permits varying levels of details or degrees of fidelity to be used in an integrated fashion. An analysis may be commenced with approximate models at each level and refined as the analysis proceeds. Furthermore, such a multi-level approach can be coupled with exergy-based synthesis/design analysis and optimization methodologies, which relate every system component and subsystem to overall system requirements in a *framework of common metrics*. The latter have received a lot of attention lately as potentially useful methods for aircraft

system/subsystem development (e.g., see [11, 12]). The advantages of exergy-based methodologies for application to aircraft systems stem from their ability to support all required levels of synthesis/design activity in a unified fashion, from conceptual comparisons through to the final configuration, leading to system-level, *best* or *optimized*[1] syntheses/designs. This approach can significantly streamline the analysis and optimization process for component/subsystem /system synthesis/design, minimize ground-based testing, and substantially reduce certification time and costs.

As a component of such a multi-level (DILGO, in particular) exergy-based approach, we examine, in the current paper, procedures that utilize high-fidelity computational fluid dynamics (CFD) exergy-based calculations to model the aerodynamics of the AFS of a modern commercial aircraft and compare the results with those obtained from lumped parameter or empirical models. The feasibility of using CFD exergy-based calculations to model the AFS is investigated by comparing the results from both calculations.

2 Formulation

The objective function is the exergy destruction rate of the AFS as a part of the overall aircraft exergy objective function. Two methods of computing the exergy destruction rate are i) empirical or lumped parameter models and ii) CFD models. Using CFD can provide more detailed and accurate results compared to lumped parameter models. In addition, we have commented on the assumed validity of lumped parameter models for a commercial aircraft, but such models may not be applicable or exist for unconventional configurations. CFD on the other hand requires significant computational resources compared to empirical methods. However, once computed over a range of parameters, CFD calculations can be re-used many times in an optimization cycle. Formulations for both models are presented in the current section.

2.1. Lumped Parameter Models

The lumped parameter models of interest provide the relationships to compute exergy destruction for transonic flight. It is assumed that the exergy destruction of the AFS is mainly due to drag. Relationships for computing drag are composed of two parts – the drag due to skin friction and the lift-induced drag. The models are obtained mainly from Raymer [13] and Hoerner [14] except where otherwise indicated. For an uncambered wing, the lift-drag relationship may be expressed as

$$C_D = K_1 C_L^2 + C_{D0},$$

where C_L is the lift coefficient, C_{D0} is the subsonic minimum drag coefficient, which can be estimated as

$$C_{D0} \equiv C_{D\min} = C_f \frac{S_{wet}}{S_{ref}}.$$

S_{wet} is the exposed surface area, S_{ref} is the reference area, and C_f is the skin friction coefficient. In addition, the lift factor, K_1, may be estimated as

$$K_1 = \frac{1}{AR \cdot e \cdot \pi},$$

where AR is the wing aspect ratio, M is the Mach number, and e is the span efficiency factor. The value of e was obtained from Raymer [13].

Subsonic Lift Slope

The lift may be computed from the slope of the lift curve, namely,

$$C_L = \alpha C_{L\alpha},$$

where $C_{L\alpha}$ is the slope of the wing lift curve and α is the angle of attack. $C_{L\alpha}$ may be estimated as

$$C_{L\alpha} = \frac{2AR\pi}{2 + \sqrt{4 + \frac{AR^2\beta^2}{\eta^2}\left(1 + \frac{\tan^2 \Lambda_{\max t}}{\beta^2}\right)}}\left(\frac{S_{\exp}}{S_{ref}}\right)F$$

where

$$\beta^2 = 1 - M^2,\ \eta = \frac{C_{l\alpha}}{2\pi/\beta},\ \text{and}\ F = 1.07(1 + d/b)^2.$$

In the above equations, $\Lambda_{\max t}$ is the sweep angle of the wing at the chord location where the airfoil is thickest; $C_{l\alpha}$ is the slope of the section lift and is taken as 2π based on thin airfoil theory; S_{exp} is the exposed wing planform; F is the fuselage lift factor, which accounts for the lift due to the interaction between the wing and the fuselage; d is the fuselage maximum equivalent diameter; and b is the wing span. The lift at zero degrees is

[1] The adjective *best* is used here to describe the synthesis/design found purely through analysis and *optimum* to describe that found through mathematical optimization.

estimated from thin airfoil theory for a cambered wing [15].

Estimation of the Skin Friction Coefficient

The component build-up method [13] is used to estimate the subsonic minimum drag from each component of the aircraft using a calculated flat-plate skin-friction coefficient, C_f, and a component form factor (FF) which accounts for the pressure drag due to viscous separation. The interference effects on the component drag are calculated as the factor Q. The subsonic parasitic drag is given as

$$C_{D0} = \frac{\sum \left(C_f FFQS_{wet} \right)_c}{S_{ref}} + C_{DMISC} + C_{DL\&P} \quad (1)$$

where $Q = 0.5\rho U_\infty^2 S_{ref}$; C_{DMISC} represents a miscellaneous drag coefficient, which accounts for the drag from components such as flaps, upsweep aft fuselage, base area, etc.; and $C_{DL\&P}$ is the drag coefficient due to leakage and protuberances. The subscript "c" indicates that the parameters within the bracket in Eq. (1) are different for each component.

The flat-plate skin friction coefficient, C_f, depends on Reynolds number, Re, and Mach number, M. The expression for a turbulent flat plate is expressed by

$$C_f = \frac{0.455}{\left(\log_{10} \mathrm{Re}\right)^{2.58} \left(1 + 0.144M^2\right)^{0.65}}, \quad (2)$$

where $\mathrm{Re} = \rho U_\infty l / \mu$, and l is the characteristic length, while U_∞ is the speed of the aircraft. For the wing, l is the mid span wing chord. For the fuselage, l is the equivalent diameter at the thickest cross-section, where the area is denoted by A_{max}.

The form factor FF can be estimated for the wing and fuselage as follows:

Wing:

$$FF = \left[1 + \frac{0.6}{(x/c)_m} \left(\frac{t}{c} \right) + 100 \left(\frac{t}{c} \right)^4 \right] \left[1.34M^{0.018} \left(\cos \Lambda_m \right)^{0.28} \right] \quad (3)$$

Fuselage:

$$FF = \left[1 + \frac{0.6}{f^3} + \frac{f}{400} \right]. \quad (4)$$

where $(x/c)_m$ is the chord-wise location of the airfoil maximum thickness, Λ_m is the sweep angle at the maximum thickness line, and f is given by

$$f \equiv \frac{l}{d} = \frac{l}{\sqrt{(4/\pi) A_{\max}}}.$$

Leaks and protuberances add drag and are difficult to predict by any method. Protuberances include antennas, lights, fuel vents, actuators, etc. These quantities are ignored as they are not included in the CFD model to which the current estimates will be compared.

Exergy Calculation

The exergy destruction rate may be computed from the overall parasitic drag [11, 12]

$$\dot{E}x_{DES}^{DRAG} = \frac{TD_{parasitic} U_\infty}{T_0}, \quad (5)$$

where T is the average temperature of the aircraft, $D_{parasitic}$ is the total parasitic drag force (which includes the pressure drag due to flow separation and lift and viscous drag due to friction), U_∞ is the speed of the aircraft, and T_0 is the reference temperature, typically taken as the "sea level" temperature.

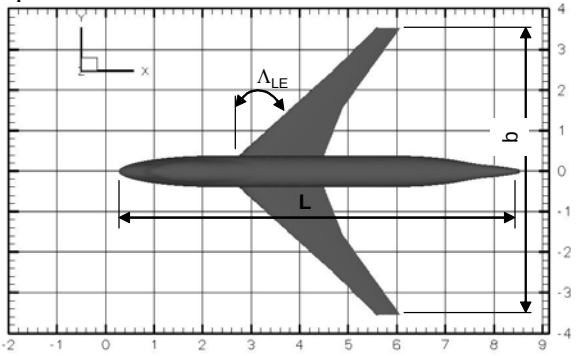

Fig. 1. Profile of the B747-200 non-dimensionalized by mid-span wing chord length, c_{mid} = 8.3261m.

Parameter values used for theAFS are shown in Table 1.

Table 1. Parameter values for the AFS empirical model.

Component	Parameter		Value
Wing	b/L	Wing span	7.5
	Λ_{LE}	Sweep angle	40°
	AR	Aspect ratio	4.98
	t/c	Thickness ratio	0.2
	x/c	Thickest point	0.24
	Λ_m	Sweep angle at maximum thickness	10°
	S_{wet}/S_{ref}	Exposed area to reference area	6.49308
	S_{ref}	Reference area (L^2)	69.324
Fuselage	l/L	Fuselage length	8.2
	d/L	Fuselage maximum diameter	0.76
	S_{ref} (m^2)	Reference area (L^2)	69.324

Based on the above equations and values as well as $M = 0.855$, $\alpha = 0^o$, and Re = 3.5 x 10^6, the friction and form factor for the components of the aircraft are

Wing
$C_f = 0.0033486$, $FF = 2.2075$,

Fuselage:
$C_f = 0.00351128$, $FF = 1.02745$,
$C_D = 0.0806$.

The drag was calculated as 293,702.53 N and the total exergy destruction rate as 8.69 x 10^7 W.

2.2 The CFD Procedure

This section describes the CFD procedure used to model the exergy destruction for the AFS. The CFD is based on solutions of the compressible Navier-Stokes equations, i.e.

$$\frac{\partial Q}{\partial t} + \frac{\partial (F - F_v)}{\partial \xi} + \frac{\partial (G - G_v)}{\partial \eta} + \frac{\partial (H - H_v)}{\partial \zeta} = 0, \qquad (6)$$

where Q is the vector of solution variables and F, G, and H are the Euler fluxes given by

$$Q = \frac{1}{J}\begin{bmatrix} \rho \\ \rho u \\ \rho v \\ \rho w \\ E \end{bmatrix}, \quad F = \frac{1}{J}\begin{bmatrix} \rho U \\ \rho u U + \xi_x p \\ \rho v U + \xi_y p \\ \rho w U + \xi_z p \\ (E + p)U \end{bmatrix}, \quad G = \frac{1}{J}\begin{bmatrix} \rho V \\ \rho u V + \eta_x p \\ \rho v V + \eta_y p \\ \rho w V + \eta_z p \\ (E + p)V \end{bmatrix}, \quad H = \frac{1}{J}\begin{bmatrix} \rho W \\ \rho u W + \zeta_x p \\ \rho v W + \zeta_y p \\ \rho w W + \zeta_z p \\ (E + p)W \end{bmatrix},$$

and (U, V, W) are the contra-variant velocity components defined as

$$\begin{aligned} U &= \xi_x u + \xi_y v + \xi_z w, \\ V &= \eta_x u + \eta_y v + \eta_z w, \\ W &= \zeta_x u + \zeta_y v + \zeta_z w \end{aligned} \qquad (7)$$

In the above equations, (u,v,w) are the velocity components in the Cartesian coordinate directions (x,y,z), ρ is the density, and p is the pressure. E is the total energy, which can be written as

$$E = \frac{p}{(\gamma - 1)} + \rho \frac{u^2 + v^2 + w^2}{2}.$$

The viscous terms F_v, G_v, and H_v in Eq. (6) have their usual meaning.

By using the implicit, approximately-factorized finite-difference algorithm of Beam-Warming and employing a Newton-like sub-iteration, we have the following algorithm:

$$\left[J^{-1^{p+1}} + \phi^i \Delta t_s \delta_\xi \left(\frac{\partial \hat{F}^p}{\partial U} - \frac{1}{\mathrm{Re}}\frac{\partial \hat{F}_v^p}{\partial U}\right)\right] J^{p+1} \times \left[J^{-1^{p+1}} + \phi^i \Delta t_s \delta_\eta \left(\frac{\partial \hat{G}^p}{\partial U} - \frac{1}{\mathrm{Re}}\frac{\partial \hat{G}_v^p}{\partial U}\right)\right] J^{p+1} \times$$
$$\left[J^{-1^{p+1}} + \phi^i \Delta t_s \delta_\zeta \left(\frac{\partial \hat{H}^p}{\partial U} - \frac{1}{\mathrm{Re}}\frac{\partial \hat{H}_v^p}{\partial U}\right)\right] \Delta U$$
$$= -\phi^i \Delta t_s \left[J^{-1^{p+1}} \frac{(1+\phi)U^p - (1+2\phi)U^n + \phi U^{n-1}}{\Delta t} - U^p \left(\left(\frac{\xi_t}{J}\right)_\xi + \left(\frac{\eta_t}{J}\right)_\eta + \left(\frac{\zeta_t}{J}\right)_\zeta\right)\right]$$
$$-\phi^i \Delta t_s \left[\delta_\xi \left(\hat{F}^p - \frac{1}{\mathrm{Re}}\hat{F}_v^p\right) + \delta_\eta \left(\hat{G}^p - \frac{1}{\mathrm{Re}}\hat{G}_v^p\right) + \delta_\zeta \left(\hat{H}^p - \frac{1}{\mathrm{Re}}\hat{H}_v^p\right)\right],$$

where

$$\phi^i = \frac{1}{1+\phi}, \Delta U = U^{p+1} - U^p.$$

The superscripts "p" and "n" denote the sub-iteration steps and the outer-loop time steps, respectively. In the above equations, (ξ, η, ς) are the curvilinear coordinate directions and Δt_s is the time step size for the sub-iterations. Either a first or second-order temporal accuracy can be obtained in the above iterative procedure by selecting $\phi = 0$ or $\phi = 1/2$. For $p = 1$, $U^p = U^n$ and $U^{n+1} = U^p$ at convergence in p.

For high-order differencing of flow fields with shock waves, the weighted essentially non-oscillatory (WENO) procedure [16] is used.

2.3 Entropy Calculation with CFD

The procedure for obtaining the entropy generation rate (directly proportional to the exergy destruction rate) from the CFD calculation is described in this section. The formulation is based on the Onsager relations [17] and must, therefore, be steady, i.e.

$$\dot{S}_{gen} = \frac{1}{T}\tau_{ij}\frac{\partial u_i}{\partial x_j} - \frac{q_k}{T^2}\frac{\partial T}{\partial x_k}, \qquad (8)$$

where the term on the left-hand side represents the entropy generation rate per unit volume. The first term on the right-hand side results from irreversibilities due to the conversion of mechanical energy into internal energy [18,19], while the second term results from irreversibilities due to heat transfer across finite temperature differences.

For the present studies, we have used eddy viscosity-type assumptions [4,20] to model the turbulent terms in Eq. (8). The average entropy generation rate per unit volume may, therefore, be expressed as

$$\bar{\dot{S}}_{gen} = \frac{1}{\bar{T}}\bar{\tau}_{ij}\frac{\partial \bar{u}_i}{\partial x_j} - \frac{\bar{q}_k}{\bar{T}^2}\frac{\partial \bar{T}}{\partial x_k},$$

where $\bar{\tau}_{ij} = (\mu + \mu_T)\left(\frac{\partial \bar{u}_i}{\partial x_j} + \frac{\partial \bar{u}_j}{\partial x_i} - \frac{2}{3}\frac{\partial \bar{u}_k}{\partial x_k}\delta_{ij}\right)$,

and

$$\bar{q}_k = -\left(\frac{\mu}{\mathrm{Pr}} + \frac{\mu_T}{\mathrm{Pr}_T}\right)\frac{\partial \bar{T}}{\partial x_k}.$$

In the above equations, μ_T is the eddy viscosity while Pr_T is the turbulent Prandtl number. The average entropy generation rate can be expressed in non-dimensional form as follows:

$$\bar{\dot{S}}_{gen} = \frac{1}{\mathrm{Re}}\frac{\mu+\mu_T}{\bar{T}}\left\{\begin{array}{l} 2\left(\frac{\partial \bar{u}}{\partial x}\right)^2 + 2\left(\frac{\partial \bar{v}}{\partial y}\right)^2 + 2\left(\frac{\partial \bar{w}}{\partial z}\right)^2 \\ -\frac{2}{3}\left(\frac{\partial \bar{u}}{\partial x} + \frac{\partial \bar{v}}{\partial y} + \frac{\partial \bar{w}}{\partial z}\right)^2 + \\ \left(\frac{\partial \bar{u}}{\partial y} + \frac{\partial \bar{v}}{\partial x}\right)^2 + \left(\frac{\partial \bar{u}}{\partial z} + \frac{\partial \bar{w}}{\partial x}\right)^2 + \left(\frac{\partial \bar{w}}{\partial y} + \frac{\partial \bar{v}}{\partial z}\right)^2 \end{array}\right\} \quad (9)$$

$$+ \frac{1}{(\gamma-1)M\,\mathrm{Re}\,\mathrm{Pr}}\frac{\mu/\mathrm{Pr} + \mu_T/\mathrm{Pr}_T}{\bar{T}^2}\left\{\left(\frac{\partial \bar{T}}{\partial x}\right)^2 + \left(\frac{\partial \bar{T}}{\partial y}\right)^2 + \left(\frac{\partial \bar{T}}{\partial z}\right)^2\right\},$$

where, for the curvilinear coordinate system used, we have that

$$\frac{\partial u_i}{\partial x_j} = \frac{\partial u_i}{\partial \xi}\xi_{x_j} + \frac{\partial u_i}{\partial \eta}\eta_{x_j} + \frac{\partial u_i}{\partial \varsigma}\varsigma_{x_j},$$

$$\frac{\partial T}{\partial x_j} = \frac{\partial T}{\partial \xi}\xi_{x_j} + \frac{\partial T}{\partial \eta}\eta_{x_j} + \frac{\partial T}{\partial \varsigma}\varsigma_{x_j}.$$

Note that integration over the volume of the entropy generation rate per unit volume is required in order to obtain the total entropy generation rate in the domain. Also note that the above formulation allows the rate of entropy generation to be computed as a derived (post-processed) quantity.

The balance for the exergy in a control volume may be expressed as [12]

$$\frac{dE_x}{dt} = \sum_{k=0}^{c}\left(1 - \frac{T_0}{T_k}\right)\dot{Q}_k - \dot{W}_S - T_0\dot{S}_{gen}^{TOTAL} + \sum_{j=1}^{IN}\dot{m}_j(e_x)_j - \sum_{j=1}^{OUT}\dot{m}_j(e_x)_j, \quad (10)$$

where

$$e_x = h - T_0 s - \mu_0 + \frac{v^2}{2} + gz, \quad (11)$$

$$E_x = E_i - T_0 S + P_0 V - \sum_{l=1}^{n}\mu_{l_0} m_l, \quad (12)$$

and h, s, μ, m, E_i, V, P_0, and T_0 are the specific enthalpy, specific entropy, specific chemical potential, constituent mass, total energy, volume, and "dead state" pressure and temperature respectively, while v and z are, respectively, the velocity and elevation of the bulk flows entering and exiting the control volume. "n" is the total number of constituents in the control volume and Q_k represents the heat loss at location "k" from the control volume. Note that the entropy generation rate which appears in Eq. (10) is that given in Eq. (8) or (9) integrated over the volume.

For steady state, the exergy storage rate in the control volume (term to the left of the equals in Eq. (10)) is zero and Eq. (10) reduces to

$$0 = \dot{E}_x^Q - \dot{W}_s - \dot{E}x_{DES} + \dot{E}x_{IN} - \dot{E}x_{OUT}, \quad (13)$$

where there is a one-to-one correspondence between the terms to the right of the equal sign in this equation and those in Eq. (10).

From the Guoy-Stodola relation, the rate of exergy destruction due to the irreversibilities occurring in a process is directly proportional via the "dead state" temperature, T_o, to the rate of entropy generation, namely,

$$\dot{I} = T_0\dot{S}_{gen}^{TOTAL} = \dot{E}x_{DES}, \quad (14)$$

For the AFS, the contributions to exergy destruction are the entropy generation due to the drag and that due to the heat loss from the airframe over a finite temperature difference, i.e.

$$\dot{E}x_{DES} = T_0\dot{S}_{gen}^{Q} + T_0\dot{S}_{gen}^{DRAG} = \dot{E}x_{DES}^{Q} + \dot{E}x_{DES}^{DRAG}. \quad (15)$$

Thus, substituting Eqs. (5) and (15) into (13) provides an expression for determining the exergy destruction rate due to heat loss from the airframe over a finite temperature difference, i.e.

$$\dot{E}x_{DES}^{Q} = \dot{E}_x^Q - \dot{E}x_{DES}^{DRAG} + \dot{E}x_{IN} - \dot{E}x_{OUT}. \quad (16)$$

The above quantities can be computed by integrating over the CFD domain. In addition, the value of net exergy flow into the CFD domain may be calculated using the expression

$$\dot{E}x_{IN} - \dot{E}x_{OUT} = \int(\rho\hat{n}\cdot\bar{u})\frac{u^2}{2}dA \quad (17)$$

Observations have shown that the contributions to the entropy generation rate due to drag in Eq. (9) show very steep gradients close to a wall and numerical simulations are far more effective with wall functions for the production terms [19,21].

This is particularly important for simulations with large values of y^+ (necessary when it is computationally impractical to resolve the flow at the wall for large CFD models). The high Reynolds number k–ε model employs wall functions in place of resolving the flow at the wall [22]. It has been used for turbulent entropy calculations [21,23].

2.4 Drag Calculation with CFD

The lift and drag coefficients may be derived from the CFD calculations using the following expressions:

$$C_L = \frac{LIFT}{0.5\rho U_\infty^2 S_{ref}}, C_D = \frac{DRAG}{0.5\rho U_\infty^2 S_{ref}}, \quad (18)$$

where

$$LIFT = F_z \cos\alpha - F_x \sin\alpha,$$
$$DRAG = F_z \sin\alpha + F_x \cos\alpha,$$

and

$$\frac{\overline{F}}{0.5\rho U_\infty^2} = \int \frac{p}{0.5\rho U_\infty^2} \cdot \hat{n} dS.$$

The skin friction coefficient may be calculated as

$$C_F = \int \frac{-\mu \frac{\partial u_\tau}{\partial n}\Big|_{wall}}{0.5\rho U_\infty^2} dS, \quad (19)$$

where the subscript "wall" indicates quantities computed on the surface of the aircraft. The total drag force can then be computed from

$$D_{Total} = \left(C_{DP} + C_f\right) 0.5\rho U_\infty^2 S_{ref}. \quad (20)$$

The rate of exergy destruction due to the drag can then be computed using Eq. (5).

3 Calculation of Flow over Boeing 747-200 Commercial Aircraft

The entropy production associated with the flow over the Boeing 747-200 commercial aircraft was calculated, as a way of generating exergy-based design data for the AFS of an integrated aircraft design/synthesis analysis. The following conditions were used: M = 0.855, α = 3.05°, reference area = 1676.4 m^2, moment center = (34, 0.0, 4.8735) m, moment reference length = 8.32612 m, and Re = 420368.7 per m. The spatial dimensions have been normalized with the moment reference length, leading to a reference Reynolds number of $Re = 3.5\times10^6$. Both Euler and Navier-Stokes calculations were carried out using a high-order discretization. The computational grids contained nine blocks with the following grid points: fuselage 138 x 70 x 30 = 416,000, nose cone 31 x 20 x 30 = 18,600, tail cap 31 x 20 x 30, wing base 129 x 38 x 30 = 147,060, wing mid section 50 x 129 x 29 = 187,050, wing tip (top) 77 x 41 x 28 = 81,508, wing tip (bottom) 77 x 41 x 28 = 81,508, wing patch 71 x 71 x 71 = 357,911, and far-field grid 73 x 39 x 48 = 136,656. This yields a total number of grid points of 1,444,993. The first grid at the wall is located approximately at Δy = 1 x 10^{-4} which corresponds to a $y^+ \approx 80$. The grid used for the calculations is shown in Fig. 2 and described below.

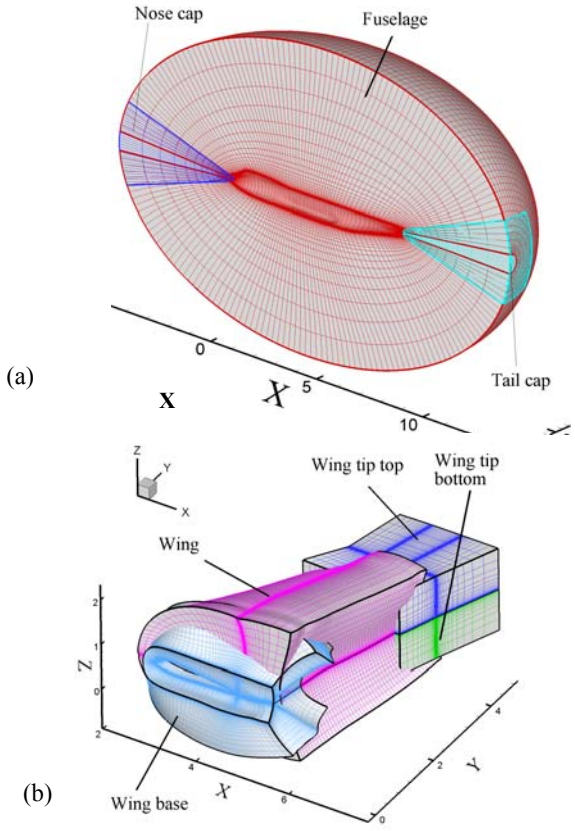

Figure 2. Mesh used for the computation of flow around the B747-200.

3.1 The B747-200 Overset Grid System

The fuselage surface is modeled using three overset blocks as shown in Fig. 2(a). Block 2 spans most of the fuselage length in the physical x-direction. Blocks 3 and 4 are designed to cover the nose and tail surfaces of the fuselage. These two

blocks are necessary to avert the computational singularities near the two poles.

Figure 2(b) shows an ensemble view of the computational grids, Blocks 5 through 8, around the wing. Block 5 (wing base) is a C-H grid designed to connect the wing and fuselage surfaces. Block 6 (wing) is a C grid and extends over most of the wing span. Blocks 7 and 8 (wing tip top and bottom) consist of the H-H topology. The computational blocks around the wing exhibit enhanced grid density near the wing trailing edge and near the wing tip. For all computational blocks near solid walls (Blocks 2 through 8), the normalized grid spacing at the wall is $\Delta = 1\times10^{-4}$.

A far-field, box-shaped grid (not shown in Fig. 2) is designed to connect the computational blocks near the fuselage and the wing with far-field conditions. For Block 1, the grids are clustered near the fuselage and wing blocks in all computational directions.

Details of the calculation and some of the difficulties encountered in performing them are presented in Ladeinde et. al. [23]. The results are discussed below.

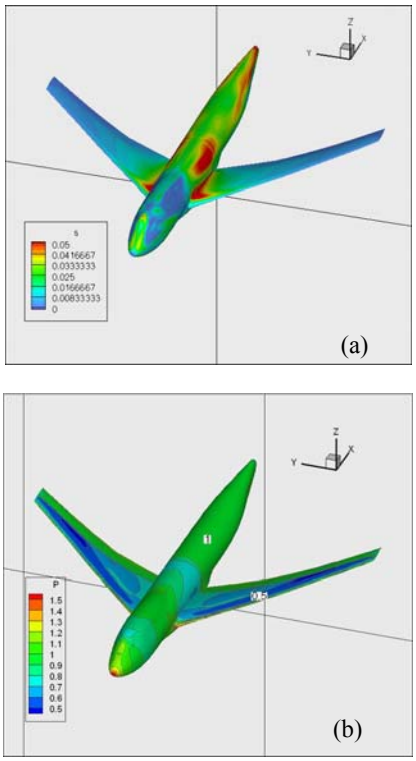

Figure 3. Contours of (a) entropy generation rate due to drag and (b) pressure around the B747-200 aircraft.

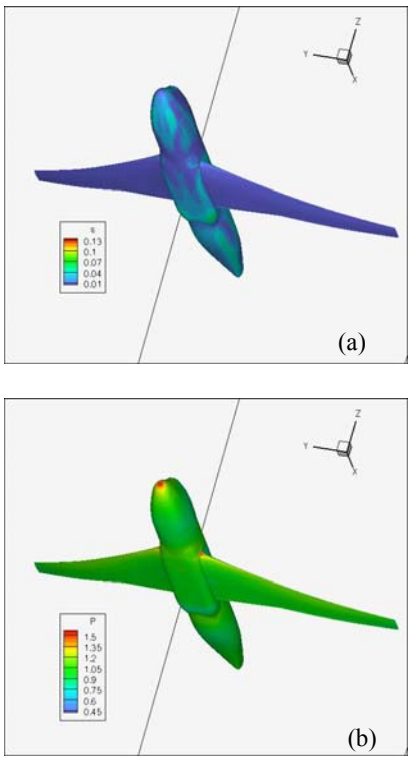

Fig. 4. Contours of (a) entropy generation rate due to drag and (b) pressure around the bottom of the B747-200 aircraft.

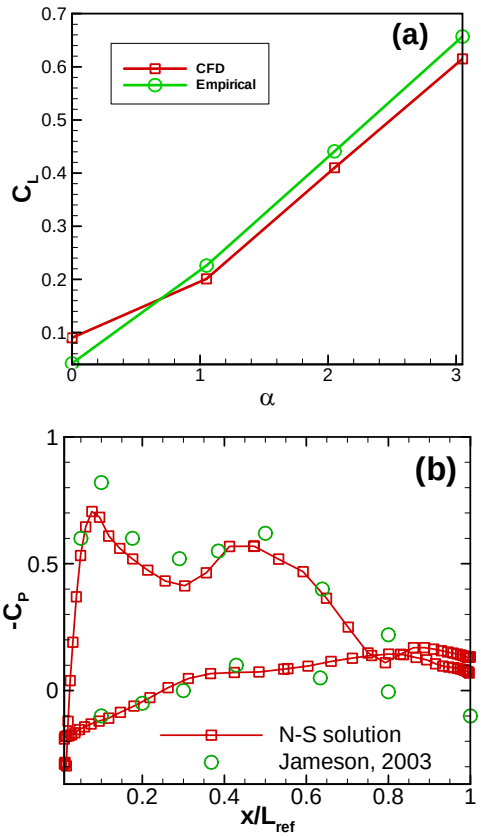

Fig. 5. Results from the B747 calculations: (a) aircraft lift curve and (b) comparisons with calculations by Jameson [23] at 42% of wing span and $\alpha = 2.05^{o}$.

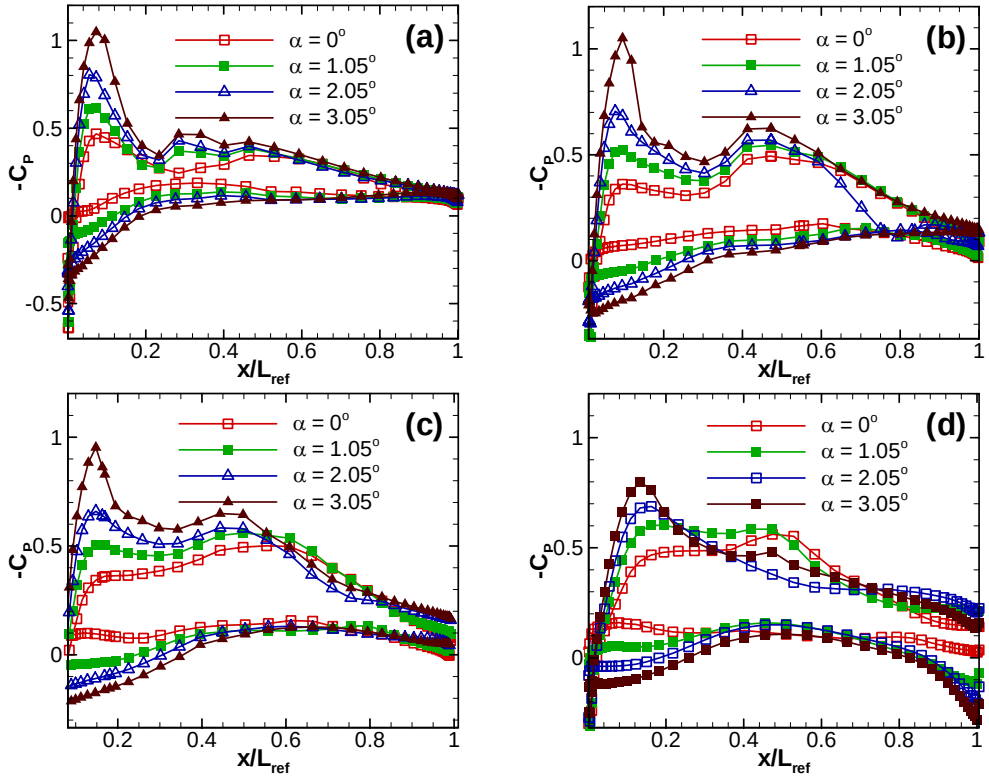

Fig. 6. Pressure coefficient compared at $0 \leq \alpha \leq 3.05$ along the wing span at locations: (a) 28%, (b) 42.9%, (c) 48.6%, and (d) 71.4%.

3.2 Results of B747-200 Calculations

Figure 3 shows the entropy generation rate due to drag and the pressure contours at the top of the fuselage and the suction side of the wing, while Fig. 4 shows the analogous plots at the bottom of the fuselage and the pressure side of the wings, respectively. From these figures, it can be seen that much of the entropy generation due to drag on the surface is generated on the top part of the plane, in the nose region and at the tip of the wing where the velocity gradients are maximum. In addition, a high entropy generation rate can be found on the fuselage just above the wings and on the wings close to the fuselage-wing junctions. On the bottom surface, most of the entropy is generated along the most curved surfaces where the velocity gradients are a maximum.

Figure 5(a) presents the lift curve obtained from the CFD calculations compared with the empirical model. Both curves show the expected nearly linear relationship between the lift coefficient and the angle of attack for small α. However, the C_L results at $\alpha = 0^o$ show a significant difference between the empirical and CFD results. The reason for this can be attributed to the approximation inherent in the lumped parameter model. In particular, we have used average zero lift values for the B747-200, even though the wing profile (thickness, camber, and camber location) varies along the wing span. Figure 5(b) includes comparisons with the inviscid calculations of Jameson [23] for the same aircraft at $\alpha = 2.05^o$. The comparisons are made at approximately 42% of wing span, with fairly good agreement. The coefficient of pressure at selected locations along the wing span is presented in Fig. 6. The curves also show a nearly linear scaling of the pressure coefficient with the attack angle for much of the wing span.

The total rate of exergy destruction over the range of angles of attack investigated is presented in Table 2 for empirical and CFD calculations. For the CFD procedure, the rate of exergy destruction from the drag, $\dot{E}x_{DES}^{DRAG}$,

given in Table 2 is that due to the pressure drag (resulting from lift and flow separation) and friction drag obtained from the CFD calculations. The rate of exergy destruction due to irreversible heat transfer, $\dot{E}x^{Q}_{DES}$, as well as the net rate of exergy flow into the domain due to mass transfer, $\dot{E}x_{IN} - \dot{E}x_{OUT}$, are also presented without comparison with the empirical procedure since the latter provides no information for quantifying them. $\dot{E}x^{Q}_{DES}$ is calculated by integrating Eq. (9) over the entire CFD domain while $\dot{E}x_{IN} - \dot{E}x_{OUT}$ is obtained by integrating Eq. (17) over the outer surface of the CFD domain. The results show that the net rate of exergy transfer into the domain increases with the angle of attack while heat transfer related rate of exergy destruction does not correlate with angle of attack.

Table 2. Comparison of exergy and aerodynamic calculations obtained via CFD and empirical relations.

CFD				
α	**0**	**1.05**	**2.05**	**3.05**
C_L	0.070	0.201	0.410	0.615
C_D (pressure induced)	0.018	0.020	0.028	0.040
C_M	-0.026	-0.023	-0.025	-0.022
C_F	0.351	0.385	0.401	0.420
Drag (N)	3.01E+05	3.30E+05	3.51E+05	3.76E+05
$\dot{E}x^{DRAG}_{DES}$ (W)	8.92E+07	9.78E+07	1.04E+08	1.11E+08
$\dot{E}x^{Q}_{DES}$ (W)	3.81E+07	3.76E+07	3.69E+07	3.73E+07
$\dot{E}x_{IN} - \dot{E}x_{OUT}$ (W)	-1.99E+06	-2.68E+06	-3.41E+06	-4.00E+06

Empirical Relations				
α	**0**	**1.05**	**2.05**	**3.05**
C_L	0.042	0.226	0.441	0.657
$K_1 C_L$	0.003	0.018	0.035	0.052
C_D (total)	0.363	0.378	0.395	0.412
Drag (N)	2.96E+05	3.08E+05	3.22E+05	3.36E+05
$\dot{E}x^{DRAG}_{DES}$ (W)	8.77E+07	9.13E+07	9.54E+07	9.96E+07

The exergy results obtained from the CFD calculations for the drag force show good agreement with those obtained from the empirical relationships, and both calculations show a similar trend with increasing angles of attack. In general, the results from the table show that when using exergy as a common metric, these calculations can just as easily and with good results be based on CFD procedures as on the empirical formulations that have typically been employed.

4 Conclusions

As a component of a multi-level or decomposition (DILGO, in particular) exergy-based approach, this paper has examined procedures that utilize high-fidelity computational fluid dynamics (CFD) exergy-based calculations to model the aerodynamics of the AFS. The exergy destruction rate contributions of the airframe subsystem (AFS) of a Boeing 747-200 aircraft are computed using the CFD approach and compared to those obtained from empirical models. The favorable comparisons for the exergy destruction rates demonstrate the feasibility of using CFD-generated data to calculate the exergy contribution of the AFS in aircraft synthesis/ design optimization.

Why an exergy-based calculation, particularly a CFD one of high fidelity, is deemed important is that as one component of a multi-level exergy-based approach, it can be shown that such an exergy-based analysis has a significant advantage over that of an energy-based approach as a tool for system synthesis/design. Even in optimization approaches, it has long been known that the use of an exergy-based approach can provide detailed information based on a common metric about why the synthesis/design is driven towards the optimum or even provide the basis for the optimization algorithm used to find the optimal synthesis/design. It has also been demonstrated elsewhere that when optimizing, there is no strict equivalency between energy- and exergy-based objectives if they are properly interpreted. Furthermore, it is when a common currency or metric such as exergy is lacking that one is unable to easily relate very different types of inefficiencies in one part of a system (such as those in the AFS-A) to those occurring in another part (such as those in the propulsion and environmental control subsystems), which points generally to the need for *exergy* as the basis for both analysis and optimization.

Acknowledgments

This work was funded by the United States Air Force under Contract FA8650-05-C-3521

via the Phase II SBIR program. The authors are very grateful to the Air Force for giving Thaerocomp the opportunity to develop innovative research tools.

References

[1] Rancruel, D. F., A Decomposition Strategy Based on Thermoeconomic Isolation Applied to the Optimal Synthesis/Design and Operation of an Advanced Fighter Aircraft System. M.S. thesis, Advisor: M. R. von Spakovsky, Mechanical Engineering Dept., Virginia Polytechnic Institute and State University, Blacksburg, VA, May 2003.

[2] Alexandrov, N. M., Kodiyalam, S. Initial Results of an MDO Method Evaluation Study. *AIAA Paper*: AIAA-98-4884., 1998

[3] Le, A., Gray, K., Baker, M. L. Building the Aerodynamics Module for the Integrated Hypersonic Aeromechanics Tool. *AIAA Paper* 2004-215. 2003.

[4] Alabi, K., Ladeinde, F., von Spakovsky, M.R., Moorhouse, D., Camberos, J., Assessing CFD Modeling of Entropy Generation for the Air Frame Subsystem in an Integrated Aircraft Design/Synthesis Procedure. *AIAA Paper* 2006-587, Jan 2006.

[5] Rancruel, D. F., von Spakovsky, M. R., A Decomposition Strategy based on Thermoeconomic Isolation Applied to the Optimal Synthesis/Design and Operation of an Advanced Tactical Aircraft System, *Energy: The International Journal*, Elsevier, in press, 2005.

[6] Munoz, J. R., von Spakovsky, M. R., The Application of Decomposition to the Large-Scale Synthesis/Design Optimization of Aircraft Energy Systems, *International Journal of Applied Thermodynamics*, June, Vol. 4, No. 2., 2001.

[7] Munoz, J. R., von Spakovsky, M. R., 2001, A Decomposition Approach for the Large Scale Synthesis/Design Optimization of Highly Coupled, Highly Dynamic Energy Systems. *International Journal of Applied Thermodynamics*, March, Vol. 4, No. 1, 2001.

[8] Rancruel, D. F., von Spakovsky, M. R. Use of a Unique Decomposition Strategy for the Optimal Synthesis/Design and Operation of an Advanced Fighter Aircraft System. *10th AIAA/ISSMO Multi-disciplinary Analysis and Optimization Conference*, Aug 30 – Sept 1, Albany New York, 2004.

[9] Rancruel, D. F., von Spakovsky, M. R., 2003, A Decomposition Strategy Applied to the Optimal Synthesis/Design and Operation of an Advanced Fighter Aircraft System: A Comparison with and without Airframe Degrees of Freedom, *International Mechanical Engineering Congress and Exposition – IMECE'2003*, ASME Paper No. 44402, N.Y., N.Y., November 2003.

[10] Rancruel, D. F., von Spakovsky, M. R., Development and Application of a Dynamic Decomposition Strategy for the Optimal Synthesis/Design and Operational/Control of a SOFC Based APU under Transient Conditions, *International Mechanical Engineering Congress and Exposition – IMECE '2005*, ASME Paper No. IMECE2005-82986, N.Y., N.Y., November 2005..

[11] Moorhouse, D. J, Hoke, C. M., Prendergast, J. P., Thermal Analysis of a Hypersonic Inlet Flow with Exergy-Based Design Methods. *International Journal of Applied Thermodynamics*, Vol. 5, No. 4, 2002.

[12] Periannan, V., von Spakovsky, M.R., and Moorhouse, D. J., Investigation of the Effects of Various Energy and Exergy-Based Figures of Merit on the Optimal Design of a High Performance Aircraft System, *International Mechanical Engineer-ing Congress and Exposition – IMECE'2006*, ASME Paper No. IMECE2006-14186, N.Y., N.Y., November 2006.

[13] Raymer, D.P. Aircraft Design: A Conceptual Approach. AIAA Education Series. 1999.

[14] Hoener, S.F. Fluid Dynamic Drag. Hoerner Fluid Dynamics. 1965

[15] Kuethe, M. A., Chow, C. Foundations of Aerodynamics. John Wiley & Sons. 1998.

[16] Shu, C.-W. Essentially Non-Oscillatory and Weighted Essentially Non-Oscillatory Schemes for Hyperbolic Conservation Laws. *NASA CR*-97-206253, *ICASE Rep*. No. 97-65., 1997

[17] Kramer-Bevan, J. S., A tool for Analysis of Fluid Flow Losses M.Sc Thesis, University of Waterloo, Canada, 1992.

[18] Bejan, A. "Entropy Generation Minimization: The Method of Thermodynamic Optimization of Finite-Time Systems and Finite-Time Processes. *CRC Press*. New York, 1996.

[19] Adeyinka, O. B. and Naterer, G. F. Modeling of Entropy Production in Turbulent Flows. *J. Fluid Eng*. Vol. 126pp. 893-899 , 2004.

[20] Moore, J., and Moore, J. G.. Entropy Production Rates from Viscous Flow Calculations, Part I. A Turbulent Boundary Layer Flow. ASME Paper 83-GT-70, *ASME Gas Turbine Conference*, Phoenix, AZ., 1983

[21] F. Kock, H. Herwig: Local Entropy Production in Turbulent Shear Flows: A High Reynolds Number Model with Wall functions, erscheint in: *Int. J. Heat Mass Transfer*, 2004.

[22] Steffen, C. J. A Critical Comparison of Several Low Reynolds Number k-ε Turbulence Models for Flow Over a Backward-Facing Step. *NASA Technical Memorandum* 106173. AIAA-93-1927, 1993.

[23] Ladeinde, F., Alabi, K., Safta, S., Cai, X., Johnson, F. The First High-Order CFD Simulation of Aircraft: Challenges and Opportunities. *AIAA Paper* 2006-1526., 2006.

[24] Jameson, A.CFD for Aerodynamic Design and Optimization: Its Evolution over the past Three Decades. *AIAA Paper*: AIAA-2003-3438. , 2003.